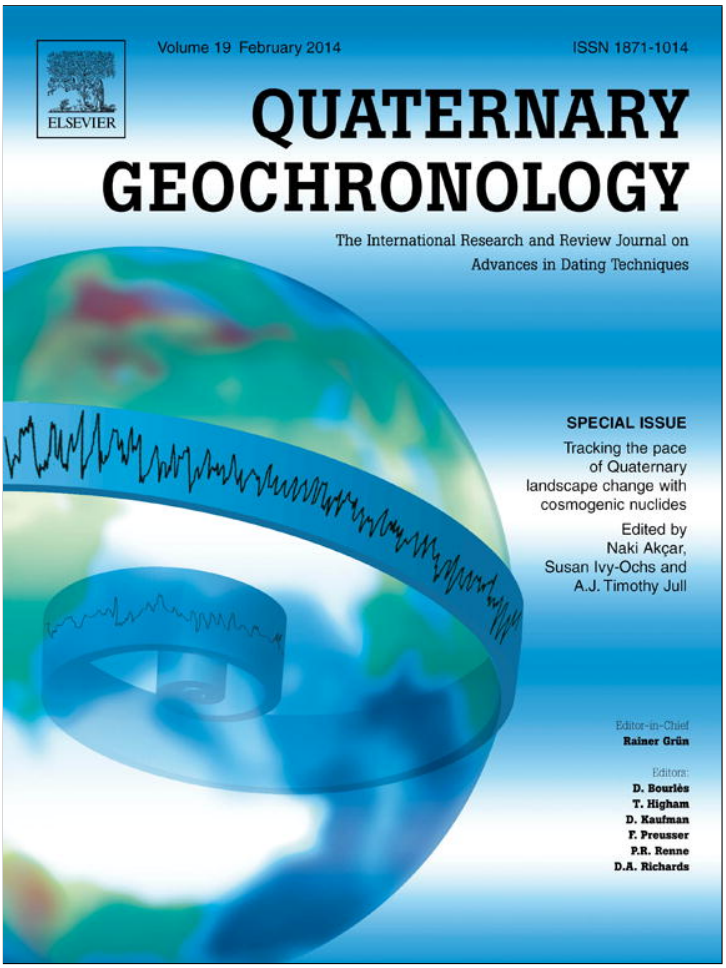

Quaternary Geochronology 19 (2014) 163–172

Contents lists available at SciVerse ScienceDirect

Quaternary Geochronology

journal homepage: www.elsevier.com/locate/quageo

Research paper

Grain size-dependent ^{10}Be concentrations in alluvial stream sediment of the Huasco Valley, a semi-arid Andes region

G. Aguilar [a,b,c,f,*], S. Carretier [a], V. Regard [a], R. Vassallo [d], R. Riquelme [e], J. Martinod [a]

[a] Geosciences Environnement Toulouse, CNRS, IRD, Université de Toulouse, France
[b] Programa de Doctorado en Ciencias Mención Geología, Universidad Católica del Norte, Antofagasta, Chile
[c] Departamento de Geología, Universidad de Atacama, Copayapu 485, Copiapó, Chile
[d] ISTerre, CNRS, Université de Savoie, 73376 Le Bourget du Lac, France
[e] Departamento de Ciencias Geológicas, Universidad Católica del Norte, Antofagasta, Chile
[f] Advanced Mining Technology Center, Facultad de Ciencias Físicas y Matemáticas, Universidad de Chile, Chile

ARTICLE INFO

Article history:
Received 17 January 2012
Received in revised form
22 January 2013
Accepted 23 January 2013
Available online 5 February 2013

Keywords:
Terrestrial cosmogenic nuclide
^{10}Be concentrations
Denudation rates
Chilean Andes
Debris flow

ABSTRACT

Terrestrial cosmogenic nuclide concentrations in sediment are used to quantify mean denudation rates in catchments. This article explores the differences between the ^{10}Be concentration in fine (sand) and in coarse (1–3 or 5–10 cm pebbles) river sediment. Sand and pebbles were sampled at four locations in the Huasco Valley, in the arid Chilean Andes. Sand has ^{10}Be concentrations between 4.8 and $8.3 \cdot 10^5$ at g^{-1}, while pebbles have smaller concentrations between 2.2 and $3.3 \cdot 10^5$ at g^{-1}. It appears that the different concentrations, systematically measured between sand and pebbles, are the result of different denudation rates, linked with the geomorphologic processes that originated them. We propose that the ^{10}Be concentrations in sand are determined by the mean denudation rate of all of the geomorphologic processes taking place in the catchment, including debris flow processes as well as slower processes such as hill slope diffusion. In contrast, the concentrations in pebbles are probably related to debris flows occurring in steep slopes. The mean denudation rates calculated in the catchment are between 30 and 50 m/Myr, while the denudation rates associated with debris flow are between 59 and 81 m/Myr. These denudation rates are consistent with those calculated using different methods, such as measuring eroded volumes.

1. Introduction

Terrestrial Cosmogenic Nuclides (TCN; e.g. ^{10}Be, ^{26}Al and ^{21}Ne) are continuously produced in the uppermost layer of the Earth's surface by the interaction between cosmic rays and matter (e.g., Lal, 1991). When the superficial denudation rate remains constant for a long time, TCN concentrations reach a steady state, and there is an inverse relationship between the TCN concentrations and the local denudation rate (Dunai and Stuart, 2009). When applied to sediment, and gathered in the river at a catchment outlet, this relationship provides a tool to quantify the mean catchment denudation rate (Brown et al., 1995; Granger et al., 1996; Bierman and Steig, 1996).

Most studies use medium to coarse sand (<1 mm) to quantify the mean denudation rate, but several studies have analyzed the TCN concentrations in distinct grain sizes finer than 1 cm, showing that they can exhibit a negative correlation between the TCN concentrations and the grain sizes (e.g. Brown et al., 1995, 1998; Insel et al., 2010; Matmon et al., 2003; Palumbo et al., 2010; Wittmann et al., 2007, 2009, 2011), a positive correlation (e.g. Heimsath et al., 2010; Hewawasam et al., 2003; Matmon et al., 2005; Palumbo et al., 2010; Ouimet et al., 2009; Wittmann et al., 2007, 2011), and even an overlapping correlation (e.g. Binnie et al., 2006; Clapp et al., 2000, 2002; Granger et al., 1996; Kober et al., 2009; Norton et al., 2008, 2011; Schaller et al., 2001; Stock et al., 2009; Wittmann et al., 2011). For more details, see the recompilation provided in the supplementary material of Codilean et al. (2012).

Only a few studies report the dependence of TCN concentrations in sediments considering grain sizes >1 cm. A negative correlation between the TCN concentrations and the grain sizes was reported by Matmon et al. (2005), a positive correlation was reported by Codilean et al. (2012) and both positive and negative correlations were reported by Belmont et al. (2007). Authors have interpreted these differences as resulting either from different hillslope processes affecting small and large grains (e.g. Brown et al., 1995, 1998; Codilean et al., 2008, 2012; Niemi et al., 2005), or from fluvial processes (Belmont et al., 2007; Carretier et al., 2009; Carretier and

* Corresponding author. Advanced Mining Technology Center (AMTC), Facultad de Ciencias Físicas y Matemáticas, Universidad de Chile, AV. Tupper 2007, piso 3, Santiago, Chile. Tel.: +56 02 9780629.
E-mail addresses: german.aguilar@uda.cl, geaguilarm@hotmail.com (G. Aguilar).

1871-1014/$ – see front matter © 2013 Elsevier B.V. All rights reserved.
http://dx.doi.org/10.1016/j.quageo.2013.01.011

Regard, 2011; Vassallo et al., 2011). However, there are very few data supporting these interpretations, in particular for pebbles and cobbles.

Yet, understanding the origin of the differences in the TCN concentrations between sand and pebbles is fundamental for at least three reasons: 1 – if hillslope or fluvial processes are able to create these differences, then comparing the TCN concentrations in sand and pebbles could provide a way to identify and quantity these different processes, provided that we know which process dominates. 2 – Sampling clasts of selected lithology in the river bed could allow us to map denudation rates for different upstream regions in a catchment. However, this requires sampling pebbles to identify the lithology, and thus, it is important to verify whether their TCN concentration is mainly controlled by the hillslope denudation rate or not. 3 – To know the best range of grain size to calculate either the erosion rates, or the exposure dating of the geomorphic markers, choosing samples with minimum inherited TCN concentrations before the construction of a geomorphic marker.

In this paper, we analyze the differences in the TCN concentration between sand and pebbles in the Huasco Valley, northern Chile, a semi-arid drainage basin (Fig. 1). This catchment is characterized by contrasting geomorphic processes, topographic patterns, and lithologies. This makes this region an exceptional laboratory for evaluating the respective effects of these factors to explain the differences in the TCN concentrations between sand

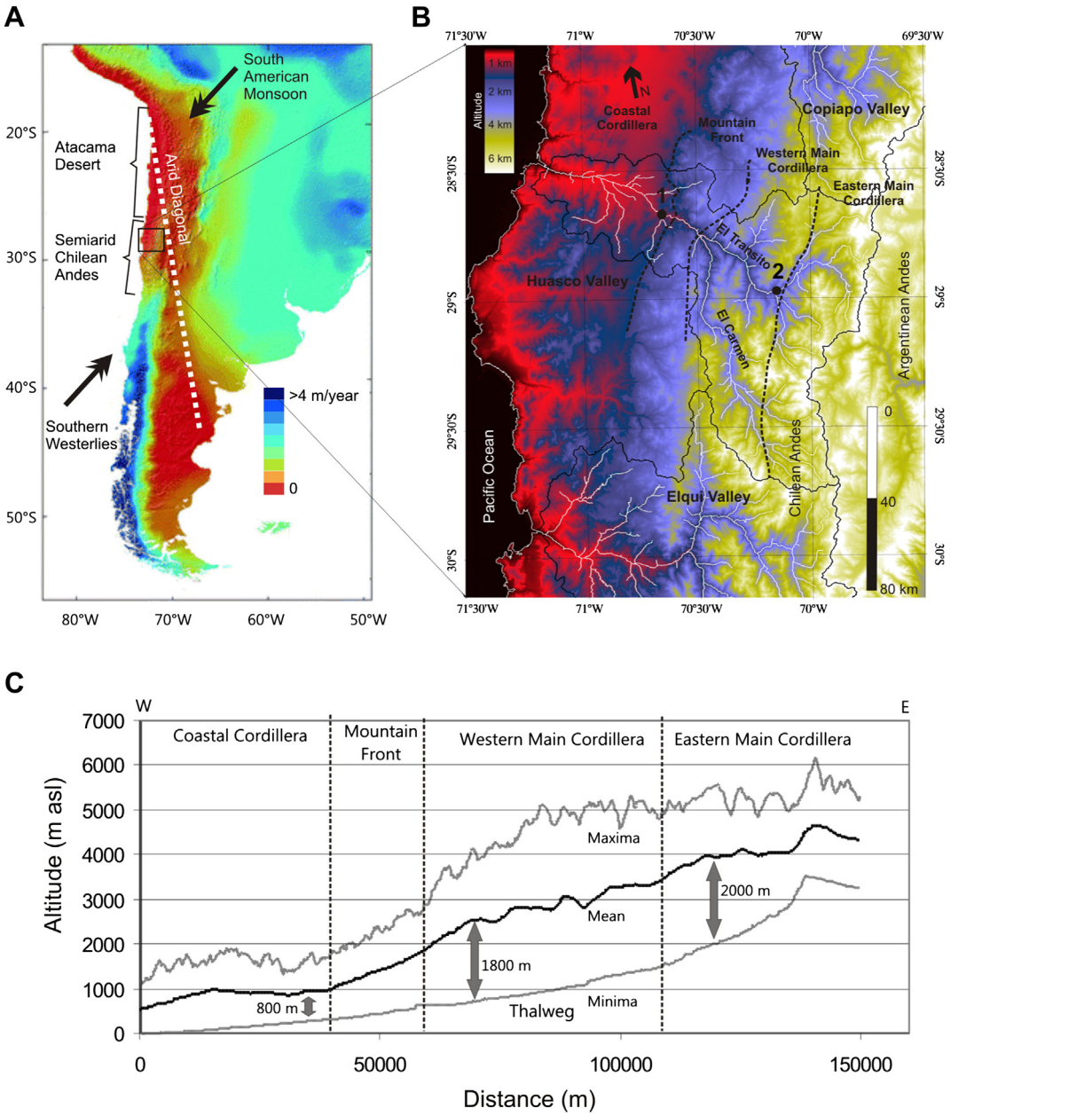

Fig. 1. A: Digital model of precipitation that show the climatic transition of the western slope of the Andes, from the hyper-arid subtropical climate of Atacama Desert to humid regions in the south (Taken and modificated from Strecker et al., 2007). B: Digital elevation model showing the geomorphic units of the semi-arid Chilean Andes: Coastal Cordillera, Mountain Front, Western Main Cordillera and Eastern Main Cordillera. The black lines mark the boundary of the main drainage basins. (1) Algodones hydrological station (700 m asl); (2) Conay meteorological station (1400 m asl). C: Minimum, mean and maximum altitude in a 150 km wide-swath along the Andean forearc at the Huasco Valley latitude. Maximum and minimum altitudes show the higher mountain peak and the Huasco trunk valley thalweg profile, respectively.

and pebbles. Our results are intended to guide future sampling methodologies in basins where variations in TCN concentrations are reported, and to refine its applicability to answer geomorphologic questions (e.g. Belmont et al., 2007; Binnie et al., 2007; Cyr and Granger, 2008; Safran et al., 2005; Vance et al., 2003; Wobus et al., 2005).

2. Regional setting

2.1. Geomorphological setting

The Huasco Valley is characterized by four longitudinal physiographic units: the Coastal Cordillera, the Mountain Front, the Western Main Cordillera and the Eastern Main Cordillera (Fig. 1). We focused our analysis on the Mountain Front and the Western and Eastern Main Cordillera. These units are mainly composed of granitic rocks from a Paleozoic intrusive-metamorphic complex, partly covered by Mesozoic–Cenozoic volcano-sedimentary successions with a predominance of andesitic rocks (Bissig et al., 2001; Martin et al., 1995).

The Mountain Front, that represents the Main Cordillera piedmont, is a very sinuous and rather degraded pediment back-scarp. Different hypsometric curves and hypsometric integral values of fluvial tributary watersheds suggest a base-level lowering of the Main Cordillera tributaries. This suggests that the Main Cordillera uplifted with respect to the Coastal Cordillera tributaries, whose base-level remained unchanged during the Neogene (Aguilar et al., 2011). In the Main Cordillera, relict pediment surfaces are preserved in the sub-horizontal inter-river areas at an elevation of ~2000 m above the river bed of the current deeply incised drainage system (Fig. 1B). The average altitude of the pediment surface is 4000 m a.s.l., rising eastward up to 5300 m a.s.l. in the Eastern Main Cordillera. The preservation of the hanging pediment surface shows that the Main Cordillera is an evolving transient landscape (Aguilar et al., 2011).

2.2. Climate setting

The semi-arid Andes region is located just south of the Arid Diagonal that crosses the Andean Cordillera at ~25°S (Fig. 1A): a transitional zone where, to the north, precipitations occur during the summer and are associated with the South American Monsoon season; whereas to the south, rainfall occurs primarily during the winter months and is associated with the Southern Westerlies (e.g. Garreaud et al., 2008). Therefore the semi-arid Andes, with a short period of winter rain between May and September (Fig. 2), represent a transitional climatic zone and rainfall regime, from the hyper-arid subtropical Atacama Desert with year-round aridity in the north, to year-round humid regions in the south. Current high water runoff and sediment fluxes reported by *Direccion General de Aguas* (General Directorate of Water) of Chile in the Huasco Valley occur at the beginning of the southern hemispheric summer which coincides with the melting of snow accumulated during the winter (Fig. 2, also see Pepin et al., 2010).

The studied region is subject to episodic high rainfall events during the ENSO years (El Niño–Southern Oscillation). Precipitation triggers exceptionally high water runoff and sediment flux (Fig. 2), in addition to the occurrence of catastrophic alluvial activations in usually arid tributary valleys (Sepúlveda et al., 2006). For instance, two torrential rainfalls (11–12/06/1997 and 16–18/08/1997) lasting for a few hours, registered the precipitation of one normal year. During the torrential rainfalls of June 1997 catastrophic debris flows developed in the lower tributary valleys (<3000 m asl) where precipitation occurred as liquid. Alluvial deposits in the outlet of tributary valleys in the Mountain Front and Western Principal Cordillera show debris flow activity during the Holocene in the Huasco Valley (Aguilar, 2010; Riquelme et al., 2010a). These deposits extend for 10 km along the tributaries. Also, the landslide deposits extend up to 7 km along the trunk valley.

Currently there is no glacial activity in the region. However glaciers occurred before 15 ky, resulting from episodes of increased moisture during the late Quaternary, that have been related to a northward shifting of the Southern Westerlies (Veit, 1996; Lamy et al., 2000) or a strengthening of the South American Monsoon resulting in the "Central Andean Pluvial Event" (CAPE, Quade et al., 2008; Riquelme et al., 2010b). Most of the erosive and depositional glacial features in the high Main Cordillera formed during these wetter periods (Ammann et al., 2001; Zech et al., 2008).

The active sediment currently leaving the catchment is a mixture of three components: (1) fluvial sediments, which are transported by the melting of snow in the Eastern Principal Cordillera, (2) debris flows that are produced during sporadic and torrential rainfalls associated to the ENSO years from the Mountain Front and Western Principal Cordillera, and (3) sediments from the gentle slopes present at the ridge crest in the whole catchment.

3. Sampling and analytic methods

We sampled sand and pebble fractions of active stream sediment in the Huasco River at four sampling points along the trunk stream (Fig. 3 and Table 1). Two sampling points are located downstream of the confluence of the Transito and Carmen valleys: one in the Coastal Cordillera and another in the Mountain Front. Two other sampling points are located in the Western Principal Cordillera: one in the Transito Valley and the other in the Carmen Valley.

One sand sample consists of approximately 2 kg of fine sediment, with diameters between 0.5 and 1 mm, sampled at 2 or 3 points located several meters away from each other and mixed together. One pebble sample consists of ca. 30 granitic rounded clasts with diameters between 1 and 3 cm (gravels) or 5 and 10 cm (cobbles) that provide a robust average concentration of ^{10}Be. Four samples were prepared in the Geociences Environnement Toulouse (GET) laboratory in Toulouse, France, following the protocol described in Von Blanckenburg et al. (1996) and adding a ^{9}Be carrier solution ($(3.025 \pm 0.009) \times 10^{-3}$ g ^{9}Be/g solution; Table 1). We used a mixture of hydrochloric and nitric acid for Quartz purification, and hydrofluoric acid for the atmospheric ^{10}Be removal. We finally obtained between 10 and 50 g of quartz (Table 1) that was dissolved using hydrofluoric acid. The other four samples were prepared in the Centre Européen de Recherche et d'Enseignement des Géosciences de l'Environnement (CEREGE) in Aix-en-Provence, France, following the protocol described in Braucher et al. (2011).

AMS measurements of the ^{10}Be concentration were performed at the French AMS National Facility, ASTER, located at CEREGE (Arnold et al., 2010). ^{10}Be data are calibrated directly versus the National Institute of Standards and Technology standard reference material NIST SRM 4325 using an assigned ^{10}Be/^{9}Be value of $(2.79 \pm 0.03) \times 10^{-11}$ (Nishiizumi et al., 2007) and a ^{10}Be half-life of $(1.387 \pm 0.012) \times 10^{6}$ yr (Korschinek et al., 2010; Chmeleff et al., 2010). Internal analytical uncertainties (reported as 1σ) include uncertainties associated with AMS counting statistics, AMS internal error (0.5%), a chemical blank measurement, and, regarding ^{10}Be, a stable measurement.

The mean ^{10}Be production rates for the Huasco Valley catchment were computed using a Digital Elevation Model (DEM) produced by SRTM data (pixel size of ~90 m) and the Stone (2000) production model. This model considers a sea level production rate of ~4.5 at g^{-1} (CRONUS; Balco et al., 2008), including the *muon*

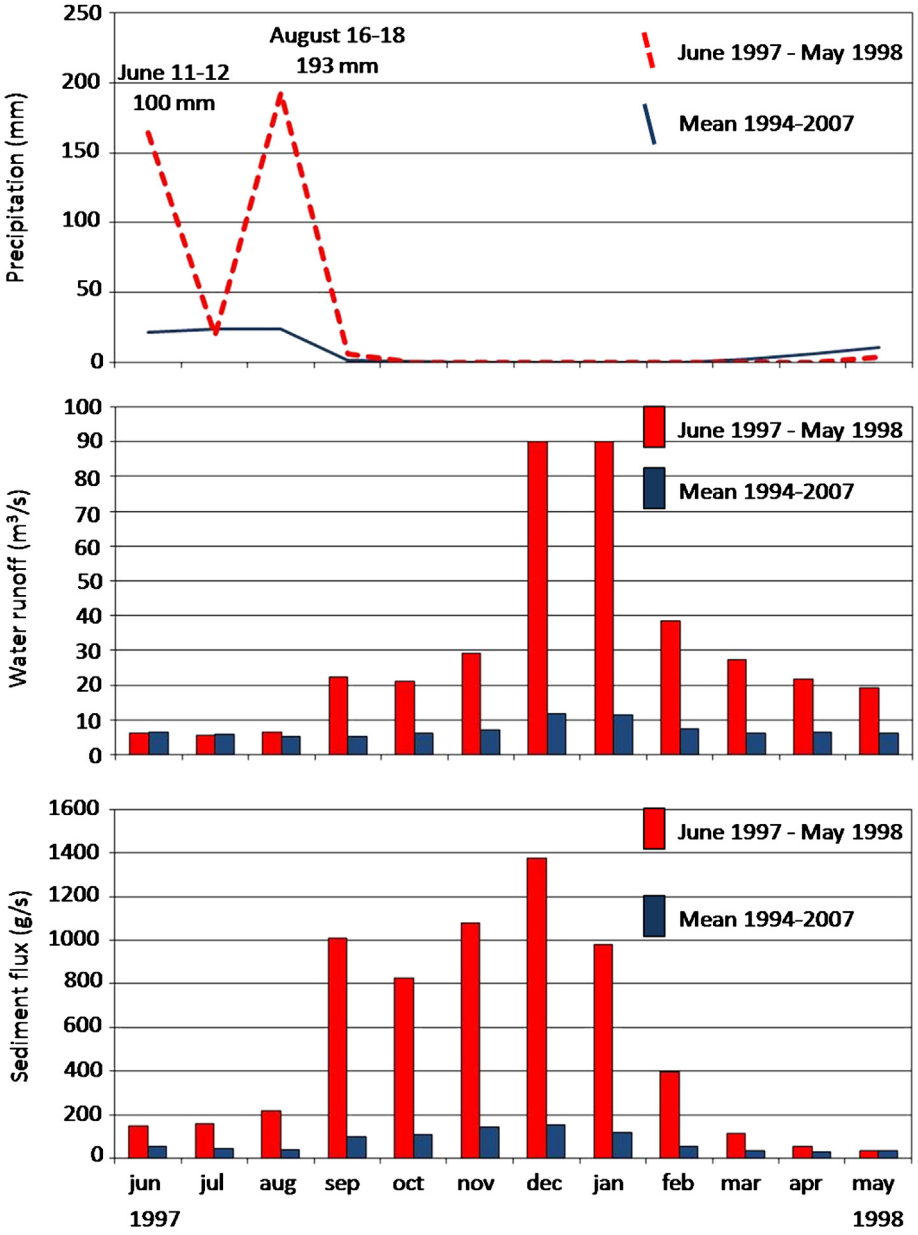

Fig. 2. Precipitation rates (lines), water runoff (bars) and sediment flux (bars) during ENSO periods of 1997–1998 (in red) and mean registered between 1994 and 2006 (in blue). Location of Algodones hydrological station (700 m asl) and Conay meteorological (1400 m asl) are shown in Fig. 1. (For interpretation of the references to colour in this figure legend, the reader is referred to the web version of this article.)

contribution (Braucher et al., 2003) and taking into account an estimate of topographic shielding for each pixel of the DEM, that turned out to be <10% (Codilean, 2006). We computed the different mean catchment production rates for distinct regions in the Huasco catchments, considering (see Fig. 2): (1) Granitic outcrops obtained from the 1/1,000,000 Geological Map of Chile (SERNAGEOMIN, 2003), (2) granitic areas with slopes >30° computed from the SRTM DEM using the slope function of GRASS, and (3) granitic areas that involve sub-catchments with evidence of Holocene debris flows, derived from the geomorphological maps presented in Riquelme et al. (2010a).

Catchment scale denudation rates were computed assuming a steady state ^{10}Be concentration on the hillslope, corresponding to an equilibrium between the rate of production of ^{10}Be atoms and their loss by surface denudation and radioactive decay (Granger et al., 1996). Furthermore, the production rates were weighted at each pixel of DEM by the relative proportion of quartz in the underlying lithology in order to limit the bias due to lithological variations (Safran et al., 2005). For each lithology, we estimated the proportion of quartz minerals from the description of lithological maps of Chile and from microscopic observations of the abundant samples collected from the Andes. The estimated proportions of quartz are: Granitoid rocks: 25%; Rhyolites: 5%; Undifferentiated detrital rocks: 5%; Ignimbrites: 2%; Other lithologies: 0%. We also computed a catchment mean production rate without correcting for the quartz content. We assume that the erosion of each lithology will produce quartz grains of similar size, and so the sand samples collected should contain detrital grains from all these lithologies. The difference between both values ranges between 2 and 18%. The error calculated for the denudation rates results from internal

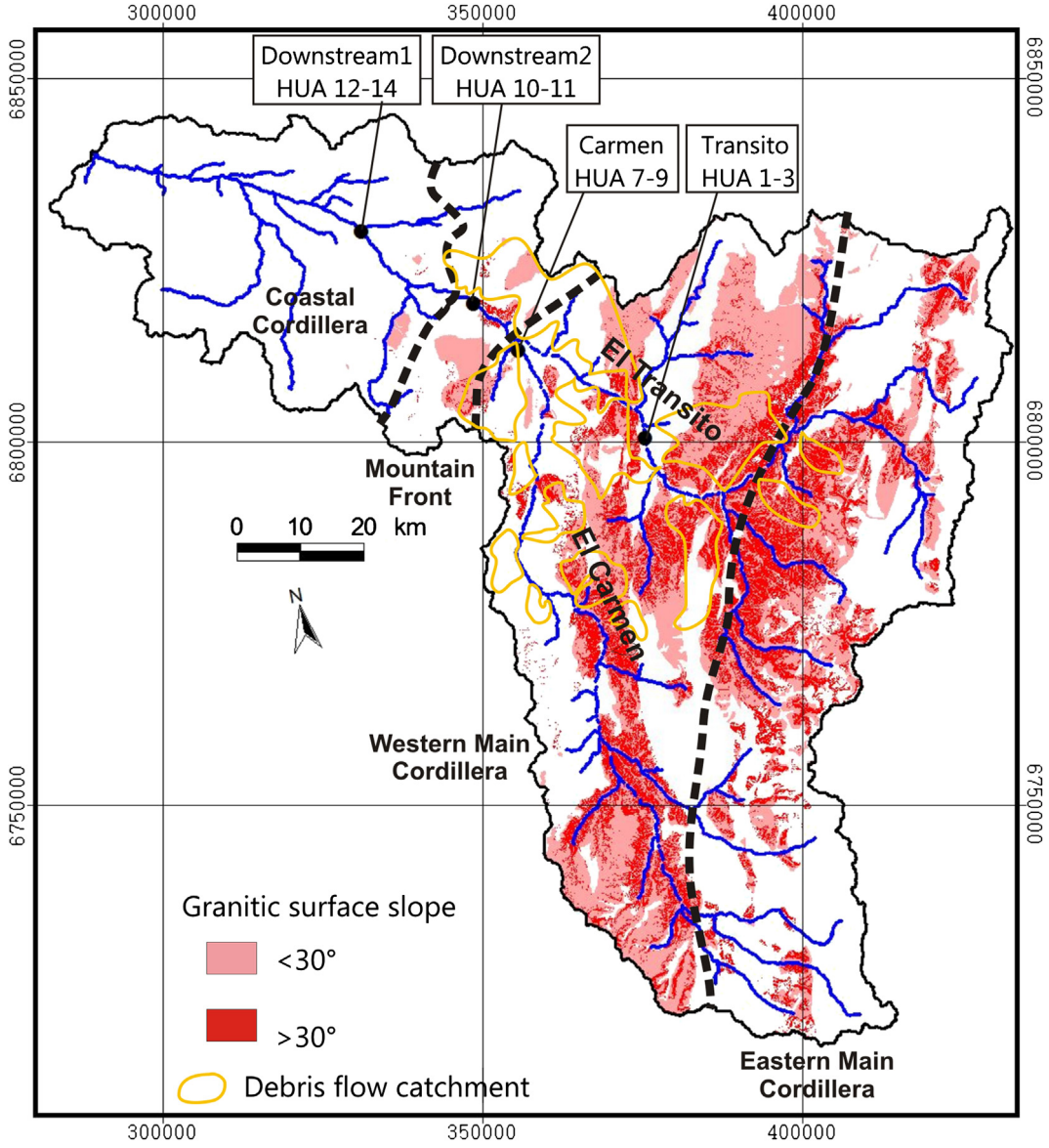

Fig. 3. Map of the Huasco Valley with sampling points within the drainage basin. Figure shows the physiographic units and the distributions of granitic surfaces in the drainage basin. Granitic surfaces are differentiated in slope degree.

Table 1
Parameters relative to analytical procedure to determine concentrations of ^{10}Be in sediments of the Huasco Valley.

Sampling position	ID	Quartz (g)	Be carrier ($g \times 10^{-6}$)	^{9}Be carrier (at $\times 10^{19}$)	^{10}Be/^{9}Be ($\times 10^{-13}$)	d^{10}Be/^{9}Be ($\times 10^{-13}$)
Transito	HUA1[a]	34.25		2.04	8.08	0.23
	HUA3[b]	13.32	308	2.38	1.86	0.08
Carmen	HUA7[a]	16.71		2.01	6.91	0.44
	HUA9[a]	20.43		2.05	3.18	0.24
Downstream2	HUA10[a]	37.35		2.03	10.80	0.30
	HUA11[b]	10.13	309	2.39	0.91	0.07
Downstream1	HUA12[b]	49.52	309	2.39	12.40	0.36
	HUA14[b]	14.69	309	2.39	1.53	0.06
CEREGE blank	RUN HUA7			1.93	0.04	0.03
	RUN HUA9			1.86	0.03	0.01
	RUN HUA1–10			2.01	0.01	0.01
GET Blank	RUN HUA3–11–12–14		307	2.37	0.005	0.004

[a] Preparation and measurement LN2C (CEREGE).
[b] Preparation GET and LN2C measurement.

Table 2
Positions of sampling points along the trunk stream of the Huasco Valley and morphometric data of catchment and granitoid surface that include: area (*A*), mean (*H*), maximum (*H*max) and minimum (*H*min) altitude, hypsometric integral (HI) and slope (*S*).

Catchment sampling position	Samples identification	Lat DD.DD (WGS 84)	Long DD.DD (WGS 84)	Catchment morphometry						Granitoid surface morphometry					
				A (km^2)	H (m)	Hmax (m)	Hmin (m)	HI	S (m/m)	A (km^2)	H (m)	Hmax (m)	Hmin (m)	HI	S (m/m)
Transito	HUA 1–3	−28.99	−70.28	3083	3591	6089	1108	0.5	0.44	1886	3455	5585	1236	0.5	0.48
Carmen	HUA 7–9	−28.80	−70.46	2876	3538	5469	853	0.6	0.45	1193	3566	5469	955	0.6	0.47
Downstream2	HUA 10–11	−28.70	−70.55	7190	3382	6089	666	0.5	0.43	3567	3396	5585	681	0.6	0.46
Downstream1	HUA 12–14	−28.60	−70.73	7343	3232	6089	434	0.5	0.42	3735	3305	5585	667	0.5	0.45

analytical uncertainties (d^{10}Be in Table 3) and a 10% external uncertainty assumed for the production rate.

4. Results: ^{10}Be concentrations in alluvial sediments

The measurements of the ^{10}Be concentrations are shown in Table 3. The ^{10}Be concentration in sand from the Carmen Valley ($(83.31 \pm 5.35) \times 10^4$ at g^{-1}) is close to the double of that from the Transito Valley ($(48 \pm 1.36) \times 10^4$ at g^{-1}). Downstream the confluence, between the Carmen and Transito valleys, intermediate concentrations are measured in sand ($(58.9 \pm 1.66) \times 10^4$ and $(59.86 \pm 2.5) \times 10^4$ at g^{-1}). In contrast, the ^{10}Be concentrations in pebbles are similar between samples from the Carmen Valley and from the Transito Valley ($(31.92 \pm 2.66) \times 10^4$ and $(33.22 \pm 1.78) \times 10^4$ at g^{-1}, respectively). Downstream the confluence, the ^{10}Be concentrations measured in pebbles are slightly lower ($(21.55 \pm 1.87) \times 10^4$ and $(24.87 \pm 1.24) \times 10^4$ at g^{-1}) than upstream of the confluence.

5. Discussion

5.1. Variability of the ^{10}Be concentrations with grain size

In the Huasco Valley, we observe a negative correlation of the ^{10}Be concentration with the sediment grain size, with a systematically lower concentration in pebbles than in sand. The corresponding ratio varies between 1.44 and 2.73 ($C_{sand}/C_{pebbles}$ in Fig. 4). A negative correlation has been observed for the medium to coarse sand (<1 mm) in several previous works (e.g. Brown et al., 1995, 1998; Insel et al., 2010; Matmon et al., 2003; Palumbo et al., 2010; Wittmann et al., 2007, 2009, 2011). In the following, we discuss the possible mechanisms explaining the systematically lower ^{10}Be concentration in pebbles (1–3 or 5–10 cm) than in sand (0.5–1 mm) from the Huasco Valley; some of these mechanisms have already been proposed by previous authors to explain the discordance in the TCN concentration when considering grain sizes >1 cm (e.g. Belmont et al., 2007; Codilean et al., 2012). These mechanisms are related to different sources or geomorphic processes in the drainage basin that control the production rates of ^{10}Be and the sediment history.

a. *Injection of glacial sediments*: Moraines of the Huasco Valley have exposure ages between 15 and 30 ka (Zech et al., 2008). Their Holocene erosion may have resulted in the injection of glacial pebbles, with probably low ^{10}Be concentrations (e.g. Wittmann et al., 2007). Glacial deposits tend to be bimodal, with many clays and coarse sediments. Then, sands may be derived from elsewhere in the catchments while pebbles may derive from low concentration glacial deposits. However, moraine outcrops represent a very small fraction of the Huasco watershed basin. For the Elqui valley, south of the study area, Carretier et al. (supplementary discussion, 2013) estimate that glacial sediment covers less than 3% of the catchment, and they conclude that the erosion of glacial sediment does not significantly impact the erosion rates calculated using cosmogenic concentrations. In the Huasco Valley, the proportion of the catchment area covered by glaciers during the Upper Pleistocene was even smaller than southward. Moreover, moraines of the Huasco catchment contain few granitic pebbles because the glaciers did not cover large granitic outcrops (Aguilar, 2010; Riquelme et al., 2010a). Then, although glacial activity may explain the smaller TCN concentrations in pebbles, we propose that another phenomenon must be invoked to explain that the TCN concentrations in sand are generally more than two times larger than in pebbles for the study area (Fig. 4).
b. *Differences in the lithological source*: Granitoid pebbles obligatorily come from granitoids, while the quartz fraction in sand may come from any source containing quartz in the drainage basin. The average production rate for drainage basins above each sample ranges between 37.2 and 41.1 at gr^{-1} yr^{-1}

Table 3
^{10}Be concentration in sand and pebbles along the trunk stream of the Huasco Valley, ^{10}Be production rates calculated considering the whole catchment area ($P_{catchment}$), only granitoid surface area ($P_{granitoid}$) and with slope >0.6 m/m ($P_{S>0.6\ m/m}$) and tributary valley area with evidence of Holocene debris flow activity ($P_{debrisflow}$), and denudation rates (E) deduced from ^{10}Be concentration in sediment. Estimated denudation rates consider production in the whole catchment area for sand and production in tributary valley area with evidence of Holocene debris flow activity for pebbles. The error of denudation rates (dE) correspond to the propagation of analytical internal uncertainties (d^{10}Be) and a 10% external uncertainty assumed for the production rate. The sand samples (0.5-1 mm) are presented in Carretier et al. (2013).

Catchment position	Sampling identification and grain fraction		^{10}Be concentration (10^4 at g^{-1})		^{10}Be production rates (at gr^{-1} yr^{-1})				Denudation rates (m/Myr)	
	ID	Grain size	^{10}Be	d^{10}Be	$P_{catchment}$	$P_{granitoid}$	$P_{S>0.6\ m/m}$	$P_{debrisflow}$	E	dE
Transito	HUA1	Sand (0.5–1 mm)	48.00	1.36	40.3	40.7	36.1	30.3	50	5
	HUA3	Cobbles (5–10 cm)	33.22	1.78					59	7
Carmen	HUA7	Sand (0.5–1 mm)	83.31	5.35	41.1	42.2	36.8	29.9	30	4
	HUA9	Gravels (1–3 cm)	31.92	2.66					61	8
Downstream2	HUA10	Sand (0.5–1 mm)	58.90	1.66	38.4	39.3	35.3	26.8	40	4
	HUA11	Cobbles (5–10 cm)	21.55	1.87					81	11
Downstream1	HUA12	Sand (0.5–1 mm)	59.86	2.50	37.2	38.2	35.3	26.2	40	4
	HUA14	Cobbles (5–10 cm)	24.87	1.24					69	8

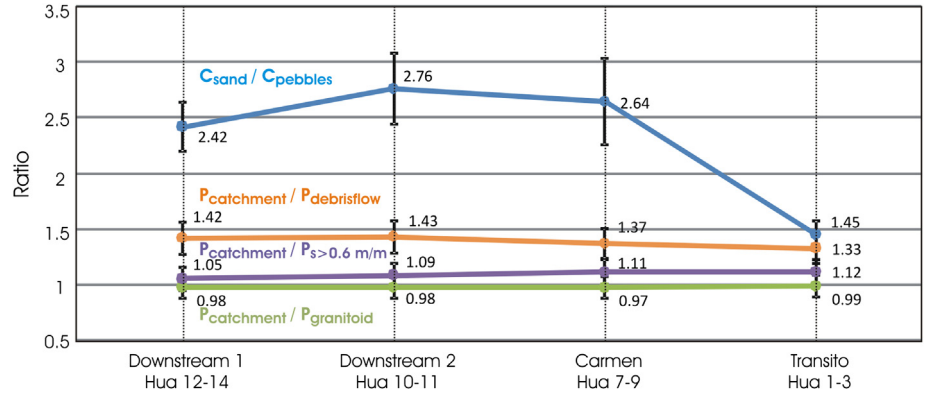

Fig. 4. Graphic that relate the ratio between ^{10}Be concentration of sand and pebbles samples ($C_{sand}/C_{pebbles}$) and the ratios between ^{10}Be production in the whole catchment and ^{10}Be production rates calculated for granitoids surface ($P_{catchment}/P_{granitoid}$), granitoids surface with slope >0.6 m/m ($P_{catchment}/P_{S\ <\ 0.6\ m/m}$) and surface with evidence of debris flow activity ($P_{catchment}/P_{debrisflow}$). See values of ^{10}Be concentration and production rates in Table 1. The error bars propagate 10% uncertainty assumed for the ^{10}Be production rate and analytical uncertainties for the ^{10}Be concentrations (d^{10}Be).

($P_{catchment}$, Table 3). Restricting the drainage basins to regions where granitoids crop out, the mean ^{10}Be production rates range from 38.2 to 42.2 at g^{-1} yr^{-1} ($P_{granitoid}$), which is similar to the production rates calculated for whole catchments. We observe this similarity because granitoid rocks are widespread in the catchment and their hypsometry is close to that of the whole catchment (see values in Table 2). Thus, different lithological provenances do not explain the observed difference between the ^{10}Be concentration ($P_{catchment}/P_{granitoid} < C_{sand}/C_{pebbles}$; Fig. 4) in pebbles and in sand.

c. *Differences in the elevation source*: Another possibility explaining the different TCN concentrations in sand and pebbles is that sand comes from the whole catchment, whereas pebbles are mainly derived from regions dominated by landslides, namely where slopes are steep (>30°, i.e. >0.6 m/m; Fig. 3), and where there are lines of evidence of Holocene debris flows (e.g. Codilean et al., 2012). The lower elevation of these sources and their greater topographic shielding result in smaller ^{10}Be production rates (e.g. Matmon et al., 2003). If only granitic surfaces with slopes >0.6 m/m are considered, the mean production rate of ^{10}Be decreases to values between 35.3 and 36.8 at g^{-1} yr^{-1} ($P_{S\ <\ 0.6\ m/m}$, Table 3). These values are only slightly lower than the ^{10}Be production rates for whole catchments. If we restrict the analysis to the area of the tributary valleys providing evidence for Holocene debris flow activity, the mean production rate of ^{10}Be further decreases to values between 26.2 and 30.3 at g^{-1} yr^{-1} ($P_{debrisflow}$, Table 3). These values, however, are still too large to explain the fact that the ^{10}Be concentrations in pebbles are half that of those in sand ($P_{catchment}/P_{debrisflow} < C_{sand}/C_{pebbles}$; Fig. 4), except in the Transito Valley where $P_{catchment}/P_{debrisflow}$(1.33) is close to $C_{sand}/C_{pebbles}$ (1.44). Thus, different elevation sources do not seem sufficient to explain the observed differences in the ^{10}Be concentration between pebbles and sand in every sampling position.

d. *Sediment attrition mechanism*: Attrition has two complementary effects that could explain why the ^{10}Be concentration is lower in pebbles than in sand. The first one is that pebbles produced in the high cordillera could be totally crushed after some travel distance in the river. Consequently, the pebbles that we gathered in the lower part of the catchment may essentially come from the lower part of the catchment, where the production rates are smaller. This process would imply that the ^{10}Be concentration in pebbles decreases downstream (Carretier et al., 2009; Carretier and Regard, 2011). However, we only observed a slight and unsystematic decrease in the ^{10}Be concentration for the pebble samples gathered downstream, which can be explained by the progressive addition of pebbles with a lower ^{10}Be concentration. This lower concentration may be due to lower production rates at lower elevations, or to higher erosion rates in the lower part of the catchment. More data are needed to corroborate this interpretation.

The second mechanism involves the random movement of boulders and sand grains within a regolith on the hillslopes. Once in the river, the boulder size decreases, and after some travel distance, it may become a pebble, corresponding to the previous boulder center. Before, on the hillslopes, this center never reached the surface, contrary to sand grains of the regolith. The mean ^{10}Be mean production rate of the sand grains (P_S) is thus larger than that of the future pebbles (P_P) (Carretier and Regard, 2011). Neglecting other production reactions than spallation, with an attenuation length of ~0.6 m, P_S/P_P is approximated by

$$P_S/P_P = [(H-2R)/H]^*[1-\exp(-H/0.6)]/[\exp(-R/0.6) - \exp(-(H-R)/0.6)], \text{with } H > 2R \quad (1)$$

where H is the regolith thickness and R is the radius of the initial boulder. The only possibility to explain a production rate ratio $P_S/P_P \approx 2$ is a regolith thicker than 10 m, and an initial boulder size of $2R \geq 1$ m. For smaller boulders, P_P tends rapidly toward P_S. A smaller H also leads to a smaller ratio. The attrition coefficient of the gathered pebbles is unknown. Nevertheless, if we refer to attrition rates $k = 0.4\%$/km determined experimentally by Attal and Lavé (2009) for granite, Steinberg's attrition law ($dR/dx = -(k/3)x$) suggests that 1 m boulders are unable to become 10 cm pebbles after 100 km travel distance. Furthermore, we do not have precise information on the thickness and distribution of the size of materials in the sediment layer on hillslopes, although 10 m seems very thick and the granitoid outcrops are generally less than 100 km away from the sampling area. Thus, it is difficult to be more conclusive on this process, which remains possible.

e. *Differences in hillslope geomorphic processes*: Hillslope geomorphic processes could have two complementary effects that may result in smaller ^{10}Be concentrations in pebbles than in sand. Pebbles could have a lower ^{10}Be concentration because they are primarily derived from the deeper layer of bedrock-involved landslides shielded from cosmic ray exposure on the

hillslopes (Brown et al., 1998). Considering an attenuation length of ~0.6 m, cosmogenic nuclide production is divided by a factor of 2 at a depth of ~0.5 m, and we know that landslides are very common in the Huasco Valley (Aguilar, 2010; Riquelme et al., 2010a). A similar interpretation is proposed by Belmont et al. (2007) to explain the low ^{10}Be concentration in gravel with respect to sand in catchments of western Washington, USA. Another simple and likely explanation is that the denudation rate in zones dominated by debris flows is larger than in the rest of the catchment (Fig. 5). A larger denudation rate would decrease the ^{10}Be concentration of pebbles produced by landslides, compared to the ^{10}Be concentration of sand produced everywhere in the catchment, particularly on the subhorizontal inter-river areas (Fig. 5), which probably erode at a smaller rate (e.g. Nishiizumi et al., 2005; Kober et al., 2009). Tributary valleys that provide evidence for Holocene debris flow activity usually cut into granitoids and therefore would be the main source of granitoid pebbles (Aguilar, 2010; Riquelme et al., 2010a). This interpretation is consistent with the observed decrease in the ^{10}Be concentration by a factor of two in sediments following low-frequency, high-magnitude debris-flow events in the Swiss Alps (Kober et al., 2012). In the Namibia Desert, in contrast, despite similar climatic conditions as in the semi-arid Chilean Andes, the TCN concentrations (including ^{26}Al and ^{10}Be) are one order of magnitude higher in quartz pebbles compared to sand (0.25–0.50 mm). Codilean et al. (2012) propose that the TCN concentration in quartz pebbles is larger because the origin of the quartz pebbles are quartz veins that are more resistant to erosion and have longer times of exposure. This different result observed in a region with a similar climate, but a smoother relief than the semi-arid Chilean Andes, shows that the dependence in the TCN concentrations with clast size is conditioned by the local and particular geomorphic processes acting on the hillslope. This observation also shows that it is very important to consider the lithology of the pebbles to interpret the TCN concentrations. In the Huasco Valley, characterized by frequent and large landslides and debris-flows as well as the preservation of wide planar segments (transient landscape), both areas, underlined by granitoids as well as differences in hillslope geomorphic processes, appear to be the more realistic explanation for the smaller ^{10}Be concentration in granitoid pebbles compared to sand.

5.2. Denudation rates in the Huasco drainage basin

We propose that the denudation rates estimated using only the ^{10}Be concentrations in sand with diameters between 0.5 and 1 mm (30 m/Myr and 50 m/Myr; Table 3) represent the mean denudation rates of all of the quartz-rich surfaces that are located upstream of the sampling points, including planar segments located in the subhorizontal inter-river areas, ~2000 m above the main river bed. This interpretation is supported by the consistency between the denudation rates calculated upstream and downstream of the confluence of the Transito and Carmen Rivers. Indeed, the denudation rate calculated from the downstream point HUA10 verifies the combination rule of the erosion rates considering the area-weighted coefficient of the catchment:

$$E_{\mathrm{HUA10}} = [E_{\mathrm{HUA7}} \times A_{\mathrm{HUA7}} + E_{\mathrm{HUA1}} \times A_{\mathrm{HUA1}}]/[A_{\mathrm{HUA7}} + A_{\mathrm{HUA1}}] = 40\mathrm{m/Ma},$$

where A denotes the quartz-rich drained area for each catchment and E is the denudation rates calculated using the ^{10}Be concentration in sand (see values in Table 3).

The integration time of the denudation rates calculated using the ^{10}Be concentration in sand is between 12 and 20 ky. Similar values are documented at a time scale of 10^6 years by calculating the eroded volumes of the tributary valleys in the high Cordillera of the Huasco Valley during the last ~8 Ma (45–75 m/Myr; Aguilar et al., 2011). The calculated denudation rates are also comparable to the Holocene denudation rates calculated using TCN concentrations in fluvial sediments in the Lluta Valley, located in the western Andean margin at 18°S (Kober et al., 2009). This supports the view that: 1. the denudation rate deduced from the ^{10}Be concentration in sand is representative of the whole catchment, and 2. the denudation rates did not vary a lot during the landscape transience in response to the Andes uplift (Aguilar et al., 2011).

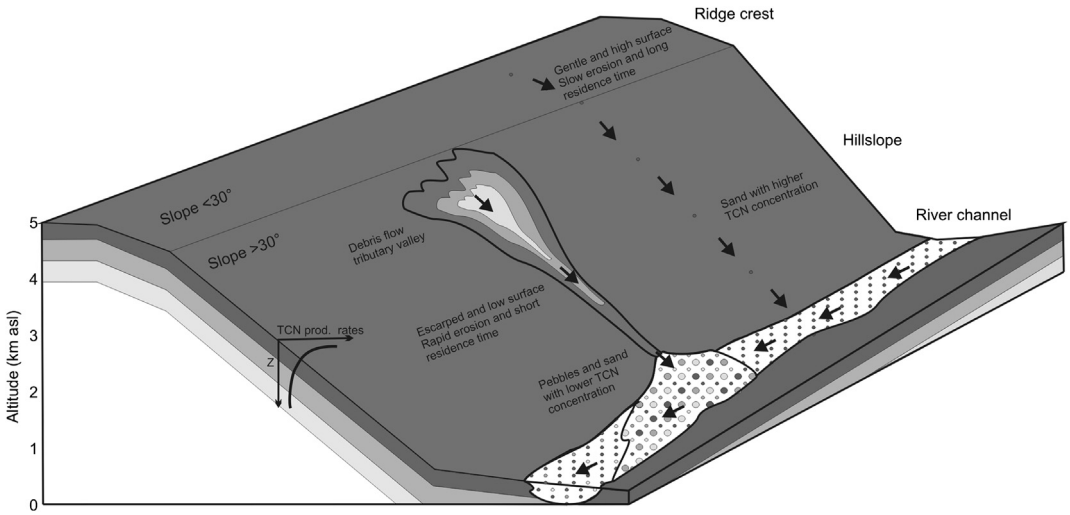

Fig. 5. Schematic diagram illustrating possible explanations for the difference in TCN concentration between sand and pebbles, involving different geomorphic processes, different sources at the surface of the hillslope and different production locations at depth (Z). Dark and light gray show high and low concentration respectively in hillslopes and in the fluvial sediment accumulated in the principal trunk valley. Escarped surfaces can be main the source of pebbles. Their rapid erosion rate associated with debris flow activity can explain low TCN concentration. On the contrary, sands are also derived from gentle and high surfaces. These surfaces have higher TCN production rate and lower erosion rates, which yield higher TCN concentrations than pebbles.

The higher denudation rate calculated for the Transito catchment compared to that of the Carmen catchment is difficult to explain. Both catchments share a similar mean slope (0.45–0.44 m/m), mean elevation (3591–3538 m) and drainage area (3083–2876 km^2) (Table 2). The only three significant differences between these catchments are: 1. The proportion of granitoid rocks: 60% of the area of the Transito catchment and 40% for the Carmen catchment. This lithological difference might explain some of the differences in the denudation rates. Nevertheless, granitoids are usually considered less erodible than other lithologies, the contrary to what our data suggest. 2. The higher maximum elevation in the Transito Valley (6089 m; Table 2). This characteristic results in higher precipitations and glacial activity resulting from the dependence of precipitation on altitude (Favier et al., 2009). 3. A smaller hypsometric integral in the Transito Valley (0.5 vs. 0.58 in the Carmen Valley; Table 2) may provide evidence for a more evolved transient landscape associated with larger denudation rates. Thus, the higher denudation rates in the Transito Valley catchment may result from the combination of several factors including glacial activity, topographical control of precipitations and a more evolved denudation history.

Our results show that granitoid pebbles present lower TCN concentrations than sand. If we accept that pebbles are mainly produced by debris flows in tributary valleys with Holocene activity of this geomorphic process (see Section 5.1), the mean denudation rates deduced from the ^{10}Be concentration and associated with this process are between 59 m/Myr and 81 m/Myr (Table 3). The integration time of the denudation rates calculated using the ^{10}Be concentration in pebbles is between 7 and 12 ky. These denudation rates may hold for the region with steep slopes (>0.6 m/m) identified in Fig. 3, which corresponds clearly to active hillslopes responding to an ongoing incision of the drainage network. In order to confirm this interpretation, the denudation rates have to be quantified in small tributaries (e.g. Kober et al., 2012) that only drain steep hillslopes.

To conclude, we suggest that the mean ^{10}Be concentration of pebbles can be used to quantify the landslide and debris flow related denudation rate, whereas the ^{10}Be concentration in sand can be used to determine the mean denudation rate of the catchment. However, to quantify the denudation rate of landslides and debris flow by the ^{10}Be concentration in pebbles, we must know the size distribution and deep of these processes in the catchments (Yanites et al., 2009).

6. Conclusion

River granitoid pebbles of the Huasco semi-arid catchment contain about half the ^{10}Be concentration of river sand. This is the third work to show a major difference between the TCN concentrations in pebbles (1–3 or 5–10 cm) and sand, and that discusses this problem. We propose that the observed difference in the TCN concentrations results from different hillslope geomorphic processes acting simultaneously, as proposed by Belmont et al. (2007) and Codilean et al. (2012) for other geomorphological contexts. One consequence of this work is that, in the Huasco Valley, pebbles should be preferred to sand when carrying out an exposure dating analysis of geomorphic markers corresponding to ancient alluvial surfaces, because the inherited TCN concentration accumulated before deposition should be lower in pebbles. This result, however, may be opposite in other geomorphological contexts and other lithologies, since Codilean et al. (2012), for instance, report a smaller TCN concentration in sand in the Namibia watershed basin that they studied. Another promising perspective of this work is that a TCN based geomorphic mapping may be performed using TCN concentrations in pebbles and the mean rates of different geomorphic processes may be quantified within a catchment, when the origin of the pebbles is identified.

Acknowledgments

This research was supported through a French project: ANR-06-JCJC-0100 ANDES and a Chilean project: INNOVA-CORFO. G. Aguilar's PhD study at the Universidad Católica del Norte and Université de Toulouse has been supported by the *Eiffel*, CONICYT, and UCN *scholarships*. The C11U02 ECOS-CONICYT project also funded research stays in France for G. Aguilar. We thank to C. Lagane for carrying out the analytic procedures in the laboratory GET-Toulouse. We thank: C. Hutchison and S. Mullin for reviewing the English content of this paper. Constructive reviews by anonymous reviewer are also acknowledged.

Editorial handling by: N. Akçar

References

Aguilar, G., 2010. Erosión y transporte de materia en la vertiente occidental de los Andes semiáridos del norte de Chile (27–32°S): desde un enfoque a gran escala temporal y espacial hasta la evolución cuaternaria de un sistema fluvial. Ph.D. thesis, Universidad Católica del Norte, Chile, y Univerisité de Toulouse, Francia.

Aguilar, G., Riquelme, R., Martinod, J., Darrozes, J., Maire, E., 2011. Variability in erosion rates related to the state of landscape transience in the semi-arid Chilean Andes. Earth Surface Processes and Landforms 36 (13), 1736–1748. http://dx.doi.org/10.1002/esp.2194.

Ammann, C., Jenny, B., Kammer, K., Messerli, B., 2001. Late Quaternary Glacier response to humidity changes in the arid Andes of Chile (18–29°S). Palaeogeography, Palaeoclimatology, Palaeoecology 172, 313–326.

Arnold, M., Merchel, S., Bourles, D.L., Braucher, R., Benedetti, L., Finkel, R.C., Aumaître, G., Gottdang, A., Klein, M., 2010. The French accelerator mass spectrometry facility ASTER: improved performance and developments. Nuclear Instruments and Methods in Physics Research Section B 268, 1954–1959.

Attal, M., Lavé, J., 2009. Pebble abrasion during fluvial transport: experimental results and implications for the evolution of the sediment load along rivers. Journal of Geophysical Research 114, 1–22.

Balco, G., Stone, J., Lifton, N., Dunai, T., 2008. A complete and easily accessible means of calculating surface exposure ages or erosion rates from ^{10}Be and ^{26}Al measurements. Quaternary Geochronology 3, 174–195.

Belmont, P., Pazzaglia, F., Gosseb, J., 2007. Cosmogenic^{10}Be as a tracer for hillslope and channel sediment dynamics in the Clearwater River, western Washington State. Earth and Planetary Science Letters 264, 123–135.

Bissig, T., Lee, J.K.W., Clark, A.H., Heather, K.B., 2001. The Cenozoic history of volcanism and hydrothermal alteration in the central Andes flat-slab region: new 40Ar-39Ar constraints from the El Indio-Pascua Au (Ag, Cu) belt, 29°20′–30°30′S. International Geology Review 43, 1–29.

Bierman, P.R., Steig, E.J., 1996. Estimating rates of denudation using cosmogenic isotope abundances in sediment. Earth Surface Processes and Landforms 21, 125–139.

Binnie, S.A., Phillips, W.M., Summerfield, M.A., Fifield, L.K., 2006. Sediment mixing and basin-wide cosmogenic nuclide analysis in rapidly eroding mountainous environments. Quaternary Geochronology 1, 4–14.

Binnie, S.A., Phillips, W.M., Summerfield, M.A., Fifield, L.K., 2007. Tectonic uplift, threshold hillslopes, and denudation rates in a developing mountain range. Geology 35 (8), 743–746.

Braucher, R., Brown, E., Bourles, D., Colin, F., 2003. In situ produced ^{10}Be measurements at great depths: implications for production rates by fast muons. Earth and Planetary Science Letters 211, 251–258.

Braucher, R., Merchel, S., Borgomano, J., Bourlès, D.L., 2011. Production of cosmogenic radionuclides at great depth: a multi element approach. Earth and Planetary Science Letters 309 (1–2), 1–9.

Brown, E.T., Stallard, R.F., Larsen, M.C., Raisbeck, G.M., Yiou, F., 1995. Denudation rates determined from the accumulation of in situ-produced ^{10}Be in the Luquillo Experimental Forest, Puerto Rico. Earth and Planetary Science Letters 129, 193–202.

Brown, E.T., Stallard, R.F., Larsen, M.C., Bourlès, D.L., Raisbeck, G.M., Yiou, F., 1998. Determination of predevelopment denudation rates of an agricultural watershed (Cayaguás River, Puerto Rico) using in-situ-produced ^{10}Be in river-borne quartz. Earth and Planetary Science Letters 160, 723–728.

Carretier, S., Regard, V., Soual, C., 2009. Theoretical cosmogenic nuclide concentration in river bed load clasts: does it depend on clast size? Quaternary Geochronology 4, 108–123.

Carretier, S., Regard, V., 2011. Is it possible to quantify pebble abrasion and velocity in rivers using terrestrial cosmogenic nuclides? Journal of Geophysical Research-Earth Surface 116 (F04003), 17. http://dx.doi.org/10.1029/2011JF001968.

Carretier, S., Regard, V., Vassallo, R., Aguilar, G., Martinod, J., Riquelme, R., Pepin, E., Charrier, R., Hérail, G., Farías, M., Guyot, J.-L., Vargas, G., Lagane, C., 2013. Slope and climate variability control of erosion in the Andes of central Chile. Geology. http://dx.doi.org/10.1130/G33735.1.

Chmeleff, J., von Blanckenburg, F., Kossert, K., Jakob, J., 2010. Determination of the ^{10}Be half-life by multicollector ICP-MS and liquid scintillation counting. Nuclear Instruments and Methods in Physics Research Section B 268, 192–199.

Clapp, E.M., Bierman, P.R., Caffee, M.W., 2002. Using ^{10}Be and ^{26}Al to determine sediment generation rates and identify sediment source areas in an arid region drainage basin. Geomorphology 45, 89–104. http://dx.doi.org/10.1016/S0169-555X(01) 00191-X.

Clapp, E.M., Bierman, P.R., Schick, A.P., Lekach, J., Enzel, Y., Caffee, M.W., 2000. Sediment yield exceeds sediment production in arid region drainage basins. Geology 28, 995–998. http://dx.doi.org/10.1130/0091-7613(2000)28<995:syespi>2.0.co;2.

Codilean, A.T., 2006. Calculation of the cosmogenic isotope production topographic shielding scaling factor for large areas using DEMs. Earth Surface Processes and Landforms 31, 785–794. http://dx.doi.org/10.1002/esp.1336.

Codilean, A.T., Bishop, P., Stuart, F.M., Hoey, T.B., Fabel, D., Freeman, S.P.H.T., 2008. Single-grain cosmogenic ^{21}Ne concentrations in fluvial sediments reveal spatially variable erosion rates. Geology 36, 159–162. http://dx.doi.org/10.1130/g24360a.1.

Codilean, A.T., Fenton, C.R., Fabel, D., Bishop, P., Xu, S., 2012. Discordance between cosmogenic nuclide concentrations in amalgamated sands and individual fluvial pebbles in an arid zone catchment. Quaternary Geochronology. http://dx.doi.org/10.1016/j.quageo.2012.04.007.

Cyr, A.J., Granger, D.E., 2008. Dynamic equilibrium among erosion, river incision, and coastal uplift in the northern and central Apennines, Italy. Geology 36, 103–106.

Dunai, T., Stuart, F., 2009. Reporting of cosmogenic nuclide data for exposure age and erosion rate determinations. Quaternary Geochronology 4, 437–440.

Favier, V., Falvey, M., Rabatel, A., Praderio, E., López, D., 2009. Interpreting discrepancies between discharge and precipitation in high-altitude area of Chile's Norte Chico region (26–32°S). Water Resources Research 45, W02424. http://dx.doi.org/10.1029/2008WR006802.

Garreaud, R.D., Vuille, M., Compagnucci, R., Marengo, J., 2008. Present-day South American climate. Palaeogeography, Palaeoclimatology, Palaeoecology. http://dx.doi.org/10.1016/j.palaeo.2007.10.032.

Granger, D., Kircher, J., Finkel, R., 1996. Spatially averaged long-term erosion rates measured from in situ-produced cosmogenic nuclides in alluvial sediment. The Journal of Geology 104, 249–257.

Heimsath, A.M., Chappell, J., Fifield, K., 2010. Eroding Australia: Rates and Processes From Bega Valley to Arnhem Land. In: Geol. Soc. Lond. Spec. Publ., vol. 346, pp. 225–241.

Hewawasam, T., Von Blanckenburg, F., Schaller, M., Kubik, P., 2003. Increase of human over natural erosion rates in tropical highlands constrained by cosmogenic nuclides. Geology 31 (7), 597–600.

Insel, N., Ehlers, T.A., Schaller, M., Barnes, J.B., Tawackoli, S., Poulsen, C.J., 2010. Spatial and temporal variability in denudation across the Bolivian Andes from multiple geochronometers. Geomorphology 122, 65–77.

Kober, F., Ivy-Ochs, S., Zeilinger, G., Schulunegger, F., Kubik, P.W., Baur, H., Wieler, R., 2009. Complex multiple cosmogenic nuclide concentration and histories in the arid Rio Lluta catchment, northern Chile. Earth Surface Processes and Landforms 34, 398–412.

Kober, F., Hippe, K., Salcher, B., Ivy-Ochs, S., Kubik, P.W., Wacker, L., Hählen, N., 2012. Debris-flow-dependent variation of cosmogenically derived catchment-wide denudation rates. Geology 40 (10), 935–938. http://dx.doi.org/10.1130/G33406.1.

Korschinek, G., Bergmaier, A., Faestermann, T., Gerstmann, U.C., Knie, K., Rugel, G., Wallner, A., Dillmann, I., Dollinger, G., Lierse von Gostomski, ch., Kossert, K., Maitia, M., Poutivtsev, M., Remmert, A., 2010. A new value for the half-life of ^{10}Be by heavy-ion elastic recoil detection and liquid scintillation counting. Nuclear Instruments and Methods in Physics Research Section B 268, 187–191.

Lal, D., 1991. Cosmic ray labeling of erosion surfaces: in situ nuclide production rates and erosion models. Earth and Planetary Science Letters 104, 424–439.

Lamy, F., Klump, J., Habbeln, D., Wefer, G., 2000. Late Quaternary rapid climate change in northern Chile. Terra Nova 12, 8–13.

Martin, M.W., Clavero, J., Mpodozis, C., Cuitiño, L., 1995. Estudio Geológico de la Franja El Indio, Cordillera de Coquimbo. Informe registrado IR-95–96, 1. Servicio Nacional de Geología y Minería, Santiago, pp. 1–238.

Matmon, A., Bierman, P.R., Larsen, J., Southworth, S., Pavich, M., Caffee, M., 2003. Temporally and spatially uniform rates of erosion in the southern Appalachian Great Smoky Mountains. Geology 31, 155–158.

Matmon, A., Schwartz, D.P., Finkel, R., Clemmens, S., Hanks, T.C., 2005. Dating offset fans along the Mojave section of the San Andreas fault using cosmogenic ^{26}Al and ^{10}Be. Geological Society of America Bulletin 117, 795–807.

Niemi, N., Oskin, M., Burbank, D., Heimsath, A., Gabet, E., 2005. Effects of bedrock landslides on cosmogenically determined erosion rates. Earth and Planetary Science Letters 237, 480–498.

Nishiizumi, K., Caffee, M., Finkel, R.C., Brimhall, G., Mote, T., 2005. Remnants of a fossil alluvial fan landscape of Miocene age in the Atacama Desert of northern Chile using cosmogenic nuclide exposure age dating. Earth and Planetary Science Letters 237, 449–507.

Nishiizumi, K., Imamurab, M., Caffee, M.W., Southon, J.R., Finkel, R.C., McAninch, J., 2007. Absolute calibration of Be-10 AMS standards. Nuclear Instruments and Methods in Physics Research Section B 258, 403–413.

Norton, K.P., von Blanckenburg, F., Schlunegger, F., Schwab, M., Kubik, P.W., 2008. Cosmogenic nuclide-based investigation of spatial erosion and hillslope channel coupling in the transient foreland of the Swiss Alps. Geomorphology 95, 474–486. http://dx.doi.org/10.1016/j.geomorph.2007.07.013.

Norton, K.P., von Blanckenburg, F., DiBiase, R., Schlunegger, F., Kubik, P.W., 2011. Cosmogenic ^{10}Be-derived denudation rates of the Eastern and Southern European Alps. International Journal of Earth Sciences 100 (5), 1163–1179.

Ouimet, W.B., Whipple, K.X., Granger, D.E., 2009. Beyond threshold hillslopes: channel adjustment to base-level fall in tectonically active mountain ranges. Geology 37, 579–582. http://dx.doi.org/10.1130/G30013A.1.

Palumbo, L., Hetzel, R., Tao, M., Li, X., 2010. Topographic and lithologic control on catchment-wide denudation rates derived from cosmogenic^{10}Be in two mountain ranges at the margin of NE Tibet. Geomorphology 117, 130–142. http://dx.doi.org/10.1016/j.geomorph.2009.11.019.

Pepin, E., Carretier, S., Guyot, J.L., Escobar, F., 2010. Specific suspended sediment yields of the Andean rivers of Chile and their relationship to climate, slope and vegetation. Hydrological Sciences Journal 55 (7), 1190–1205.

Quade, J., Rech, J.A., Betancourt, J.L., Latorre, C., Quade, Rylander, K.A., Fisher, T., 2008. Paleowetlands and regional climate change in the central Atacama Desert, northern Chile. Quaternary Research 69, 343–360.

Riquelme, R., Aguilar, G., Jensen, A., Verdejo, J., Herrera, S., Riveros, K., Navarrete, P., 2010a. Evaluación hidrogeológica de la Cuenca del Río Huasco, con énfasis en la cuantificación de los recursos hídricos superficiales y subterráneos (geomorfología, dinámica fluvial reciente y relleno de la cuenca), Informe Innova Chile, CORFO, Gobierno de Chile 5, p. 140.

Riquelme, R., Rojas, C., Aguilar, G., Flores, P., 2010b. Late Pleistocene–Early Holocene paraglacial and fluvial sediment history in the Turbio valley, semiarid Chilean Andes. Quaternary Research. http://dx.doi.org/10.1016/j.yqres.2010.10.001.

Safran, E.B., Bierman, P.R., Aalto, R., Dunne, T., Whipple, K., Caffee, M., 2005. Erosion rates driven by channel network incision in the Bolivian Andes. Earth Surface Processes and Landforms 30, 1007–1024.

Schaller, M., von Blanckenburg, F., Hovius, N., Kubik, P.W., 2001. Large-scale erosion rates from in situ-produced cosmogenic nuclides in European river sediments. Earth and Planetary Science Letters 188, 441–458. http://dx.doi.org/10.1016/s0012-821x(01) 00320-x.

Sepúlveda, S.A., Rebolledo, S., Vargas, G., 2006. Recent catastrophic debris flows in Chile: geological hazard, climatic relationships and human response. Quaternary International 158, 83–95.

SERNAGEOMIN, 2003. Mapa Geológico de Chile: versión digital. Servicio Nacional de Geología y Minería, Santiago. Publicación Geológica Digital, No. 4 (CD-ROM, versión 1.0, 2003).

Stock, G.M., Frankel, K.L., Ehlers, T.A., Schaller, M., Briggs, S.M., Finkel, R.C., 2009. Spatial and temporal variations in erosion from multiple geochronometers: Wasatch Mountains, Utah, USA. Lithosphere 1, 34–40,. http://dx.doi.org/10.1130/L15.1.

Stone, J., 2000. Air pressure and cosmogenic isotope production. Journal of Geophysical Research 105, 23753–23759.

Strecker, M.R., Alonso, R., Bookhagen, B., Carrapa, B., Hilley, G.E., Sobel, E.R., Trauth, M.H., 2007. Tectonics and climate of the Southern Central Andes. Annual Review of Earth and Planetary Sciences 35, 747–787,. http://dx.doi.org/10.1146/annurev.earth.35.031306.140158.

Vance, D., Bickle, M., Ivy-Ochs, S., Kubik, P.W., 2003. Erosion and exhumation in the Himalaya from cosmogenic isotope inventories of river sediments. Earth and Planetary Science Letters 206 (3–4), 273–288.

Vassallo, R., Ritz, J.F., Carretier, S., 2011. Control of geomorphic processes on ^{10}Be concentrations in individual clasts: complexity of the exposure history in Gobi-Altay range (Mongolia). Geomorphology 135, 35–47. http://dx.doi.org/10.1016/j.geomorph.2011.07.023.

Veit, H., 1996. Southern Westerlies during the Holocene deduced from geomorphological and Pedological studies in the Norte Chico, northern Chile (27–33°S). Palaeogeography, Palaeoclimatology, Palaeoecology 123, 107–119.

Von Blanckenburg, F., Belshaw, N.S., O'Nions, R., 1996. Separation of ^{9}Be and cosmogenic^{10}Be from environmental materials and SIMS isotope dilution analysis. Chemical Geology 129, 93–99.

Wittmann, H., von Blanckenburg, F., Guyot, J.L., Maurice, L., Kubik, P.W., 2009. From source to sink: preserving the cosmogenic^{10}Be-derived denudation rate signal of the Bolivian Andes in sediment of the Beni and Mamoré foreland basins. Earth and Planetary Science Letters 288 (3–4), 463–474.

Wittmann, H., von Blanckenburg, F., Kruesmann, T., Norton, K.P., Kubik, P.W., 2007. Relation between rock uplift and denudation from cosmogenic nuclides in river sediment in the Central Alps of Switzerland. Journal of Geophysical Research-Earth Surface 112 (F4).

Wittmann, H., von Blanckenburg, F., Maurice, L., Guyot, J.L., Filizola, N., Kubik, P.W., 2011. Sediment production and delivery in the Amazon River basin quantified by in situ-produced cosmogenic nuclides and recent river loads. Geological Society of America Bulletin 123, 934–950. http://dx.doi.org/10.1130/B30317.1.

Wobus, C., Helmsath, A., Whipple, K., Hodges, K., 2005. Active out-of-sequence thrust faulting in the central Nepalese Himalaya. Nature 434, 1008–1011.

Yanites, B.J., Tucker, G.E., Anderson, R.S., 2009. Numerical and analytical models of cosmogenic radionuclide dynamics in landslide-dominated drainage basins. Journal of Geophysical Research-Earth Surface 114. http://dx.doi.org/10.1029/2008JF001088.

Zech, R., May, J.H., Kull, C., Ilgner, J., Kubik, P.W., Veit, H., 2008. Timing of the late Quaternary glaciation in the Andes from ~15 to 40°S. Journal of Quaternary Science 23, 635–647.